Food Packaging and Shelf Life 19 (2019) 104–113

Contents lists available at ScienceDirect

Food Packaging and Shelf Life

journal homepage: www.elsevier.com/locate/fpsl

Nano silica-carbon-silver ternary hybrid induced antimicrobial composite films for food packaging application

Manik C. Biswas[a], Boniface J. Tiimob[a], Woubit Abdela[b], Shaik Jeelani[a], Vijaya K. Rangari[a,*]

[a] Department of Materials Science and Engineering, Tuskegee University, AL, 36088, United States
[b] Department of Pathobiology, Tuskegee University, AL, 36088, United States

ARTICLE INFO

Keywords:
Rice husk
Silica-carbon-silver NPs
Nanocomposites thin films
Food packaging

ABSTRACT

In this work, Ag assisted biobased silica-carbon nanoparticles (SCAg-NPs) were incorporated into a viscous biopolymer solution to fabricate antimicrobial thin films using 3D printing technique. The Ag NPs were prepared *in situ* from $AgNO_3$ through one-step ball milling in the presence of silica-carbon hybrid obtained from pyrolysis of rice husk. The nanostructure of the SCAg-NPs was determined by XRD and TEM. These as-synthesized particles were also characterized by XPS analysis. The printed films were characterized by XRD, FE-SEM, Raman microanalysis, TGA, DSC and tensile testing to investigate the influence of nanoparticles on the thermal and mechanical properties on the films. Antimicrobial testing was carried out on the films to assess the inhibitory effect of SCAg NPs on *Salmonella Enteritidis* inoculum. XRD, XPS and Raman microanalysis confirmed the incorporation of Ag particles into SCNPs, while FE-SEM size measurement of the SCAg NPs ranged between 10–100 nm in diameter. Thermal analysis revealed that the inclusion of SCAg NPs led to improvement in the thermal stability of the fabricated nanocomposites films. Tensile test was carried out to determine the influence of SCAg NPs on mechanical properties of the films and found moderate increase in the strength of the polymer film.

1. Introduction

The demand of high quality and safe food products coupled with environment concerns prompt the development of biodegradable coatings and fillers as an alternative of synthetic preservatives. Edible coating materials which are developed from generally recognized as safe (GRAS) materials can potentially enhance food freshness, appearance and integrity. Antimicrobial films and coatings has immerged as a new concept of active packaging and have been developed to reduce, inhibit, or delay the growth of microorganisms on the surface of food in contact with the package (Banaguer et al., 2013; Beigmohammadi et al., 2016; Llana-Ruiz-Cabello et al., 2015; Tornuk, Hancer, Sagdic, & Yetim, 2015; Wen et al., 2009). The use of antimicrobials packaging films to control the growth of microorganisms in food has a potential impact on shelf-life extension and food safety (Beltrán, Valente, Jiménez, & Garrigós, 2014, Beltrán et al., 2009, Moreira, Pereda, Marcovich, & Roura, 2011; Martínez-Abad, Lagaron, & Ocio, 2012; McCluskey et al., 2009; Tang et al., 2015; Wang et al., 2013). Many organic microbial active agents are available and can impart antimicrobial activity in active packaging materials. Example are chitosan (Moreira et al., 2011; Soysal et al., 2015), nisin (Soysal et al., 2015), Rhodanine (Tang et al., 2015), proallium (Llana-Ruiz-Cabello et al., 2015) and cinnamaldehyde (Balaguer, Lopez-Carballo, Catala, Gavara, & Hernandez-Munoz, 2013).

Recently, several attempts have been carried out to fabricate food packaging films integrated with high mechanical, thermal, barrier and antimicrobial effect with the intention of increasing food quality, integrity, stability and shelf life. Among the mostly used antimicrobial agents, silver nanoparticles (Ag NPs) and their salts (e.g. $AgNO_3$) exert tremendous antimicrobial potential due to its effectiveness to broad spectrum of antimicrobial activities against bacteria, virus, algae, parasites and fungi and have been widely used to fabricate food packaging films. In addition, silver nanoparticles can enhance the mechanical, thermal and barrier properties of the films. In this study, we tried to incorporate Ag NPs into the composite films and investigate the antimicrobial activity against food borne pathogens. The Ag NPs can interaction with amino acids leading to the disruption of ATP production and Ag^+ ions can affect DNA replication. Besides, reactive oxygen species (ROS), generated from Ag NPs can also have antimicrobial effect. And Ag NPs can get attach to the bacterial cell membrane causes leakage of cell components and interference of respiratory system eventually the death of the bacteria (Marambio-Jones & Hoek, 2010;

* Corresponding author.
E-mail address: vrangari@tuskegee.edu (V.K. Rangari).

https://doi.org/10.1016/j.fpsl.2018.12.003
Received 7 March 2018; Received in revised form 14 November 2018; Accepted 13 December 2018

Palza, 2015; Park et al., 2009; Pelgrift & Friedman, 2013).

Several composites have been developed integrated with reinforcing compounds to biopolymers to enhance their mechanical, thermal and barrier properties. Macroscopic reinforcing compounds have poor interaction with the matrix results biocomposites with defects. In this study, silica and carbon nanoparticles (SC NPs), widely used material in polymer industries, were used as filler materials. This is due to their large surface area, and minuscule particle size (5–20 nm) (Ma et al., 2012). Their nanoscale size and larger relative surface area to volume ratio than their conventional forms results enhanced strength and chemical reactivity. Nano-silica (SiO_2) can be fabricated by different methods. Several authors have reported different synthetic methods for producing silica from rice husk (Li, Shirai, & Fuji, 2013; Ma et al., 2012; Shen, Zhao, & Shao, 2014; Thuc & Thuc, 2013; Yuvakkumar, Elango, Rajendran, & Kannan, 2014;). Rice husk, an excellent source of silica and carbon, is produced as a primary agricultural by-product (biomass) which accounts for an average of 20% (w/w) agro-based waste (Thuc & Thuc, 2013) has been used to synthesis silica and carbon hybrid nanomaterials. Here we tried to fabricate silica-carbon-silver ternary hybrid polymeric composite films to enhance the mechanical and thermal properties of the composite films, which is due to silica-carbon hybrid nanoparticles with promising antimicrobial effect due to Ag NPs, for food packaging application through nanocomposites approach. Nanocomposites approach allows to work in nano scale range of about 1–100 nm. Due to their (SCAg-NPs) minuscule size, they have proportionally larger surface area than their micro or macroscale counterpart does.

Therefore, the prime goal of this work is to synthesis and characterization of nanomaterials from agricultural biomass and investigate the microbial activity of silver nanoparticles by making micron thick bio films using 3D printing process.

2. Materials and processing

2.1. Materials

The Ecoflex was supplied by BASF Corporation, Villa Park, IL, USA as research sample. The precursor of nano silica and carbon particles, rice husk (RH), from the Three H's, LLC Crossett, Arkansas, was used for this study. Silver Nitrate was used as the precursor for silver nanopartilces. The organic solvent Chloroform (HPLC grade, $CHCl_3$, ≥ 99%) was used to dissolve the polymer pellets with the addition of SCAg NPs, Methanol (≥ 99%), Polypropylene Glycol (PPG), Ethanol (CH_3CH_2OH), Silver Nitrate ($AgNO_3$) were obtained from Sigma Aldrich St. Louis, MO. Muller Hinton Agar (MHA), Tryptic Soy Broth (TSB) and Tryptic Soy Agar (TSA) were purchased from Acumedia Neogen Corporation, MI, USA. *Salmonella Enteritidis* (S. Enteritidis) was obtained from American Type Culture Collection (ATCC), Manassas, VA, USA.

2.2. Preparation of rice husk powder (RHP)

The as obtained RH was first washed with distilled water to remove dirt and foreign particles and then dried at 120 °C for 24 h. The dried RH was then ball milled at a ball to powder ratio of 8:1 for 3 h using stainless steel ball milling canister and 10 mm stainless steel balls shown in Fig. 1a.

2.3. Synthesis of SCNPs using pyrolysis

The prepared RHP was taken (10 g) into the vertical reaction chamber of the Ni-based superalloy high-pressure hydrothermal reactor (GSL-1100X-RC). Then the vertical reactor heated using a temperature controlled furnace. The furnace first heated to 1000 °C at a rate of 10 °C/min ramp and then hydrothermal treatment of RHP was carried out for 2 h under self-pressurized condition. After hydrothermal treatment, the as-obtained rice husk char (60% yields) was then mortared gently to make rice husk ash (RHA) at uniform size powder. The RHA contains 52% CO_2 and 48% SiO_2 confirmed by TGA analysis in presence of Oxygen.

2.4. Synthesis of SCAg NPs by ball milling

A solution of ethanol and water was prepared at 1:1 (v/v) ratio and took 20 ml in stainless steel ball milling canister. Then mixer of SCNPs/$AgNO_3$ as 1:0.2 wt. ratio was added to the stainless steel canister with the addition of 1 ml polypropylene glycol (PPG). The ball milling process was carried out for 9 h shown in Fig. 1b. After the reaction the solution was filtered and dried to get the final product.

2.5. Preparation of SCAg NPs induced composites films

The biobased nano silica-carbon-silver particles were dispersed at 0.5–1.5 wt. % to the polymer solution using ultrasound mixing for 30 min. The polymer solution was prepared by dissolving the polymer pellets in chloroform with continues magnetic stirring until the clear solution is formed. This polymer solution was used to fabricate the thin films through 3D printing process. The HYREL SYSTEM 30 M model 3D printer was used for printing process. The laser head with 201000 series Luer Tip Kit of 14 G SS was used at a feed rate of 3500 nL/s. There was no external heat to the hot bed. The films were dried at room temperature. AutoCAD software was used to make the structure and then slice the structure to create the machine readable G code file. After that, Repetrel software was used to print the structure using G code file. A schematic flow diagram of 3D printing process showed in the below Fig. 2.

3. Experimental methods

3.1. X-Ray diffraction (XRD) analysis

X-Ray diffraction (XRD) analysis was carried out using Rigaku DMAX 2100 diffractometer with monochromatic CuK α radiation (γ = 0.154056 nm) at 40 kV and 30 mA. The diffraction data for the nanomaterials of RH ash were collected from 0 to 80° of 2θ at a scan rate of 2° 2θ per minute. The analysis was carried out to analyze the phase composition of the fabricated thin films. The X-ray pattern of the as-synthesized sample is compared with the Jade library Joint committee on powder diffraction standards (JCPDS) card (file No 47-1743).

3.2. Raman spectroscopy

Raman spectroscopic analysis was carried out by DXR Raman Spectroscopy (Thermo Scientific) to understand the chemical structure of the polymer and nanoparticles. A 532 nm (5 0.0 mW power) wavelength laser was used in the Raman spectrometer to analyze the sample. The data acquisition has carried out in a range of 100-3500 cm^{-1} by OMNIC software.

3.3. BET surface area analyzer

The specific surface area of SCAg NPs was calculated using the BET method based on the nitrogen adsorption/desorption isotherms, which were produced by an automatic surface area and pore size distribution analyzer (NOVA 2200e, Quantachrome) at liquid nitrogen temperature. The sample was first degassed under vacuum at 200 °C for 1 h. After outgassing, the sample was backfilled with Helium gas to cool down and took the weight of dry outgassed sample.

3.4. X-ray photoelectron spectroscopy (XPS)

The chemical composition of the synthesized nanoparticles were investigated using X-ray photoelectron spectroscopy (XPS), a Thermo

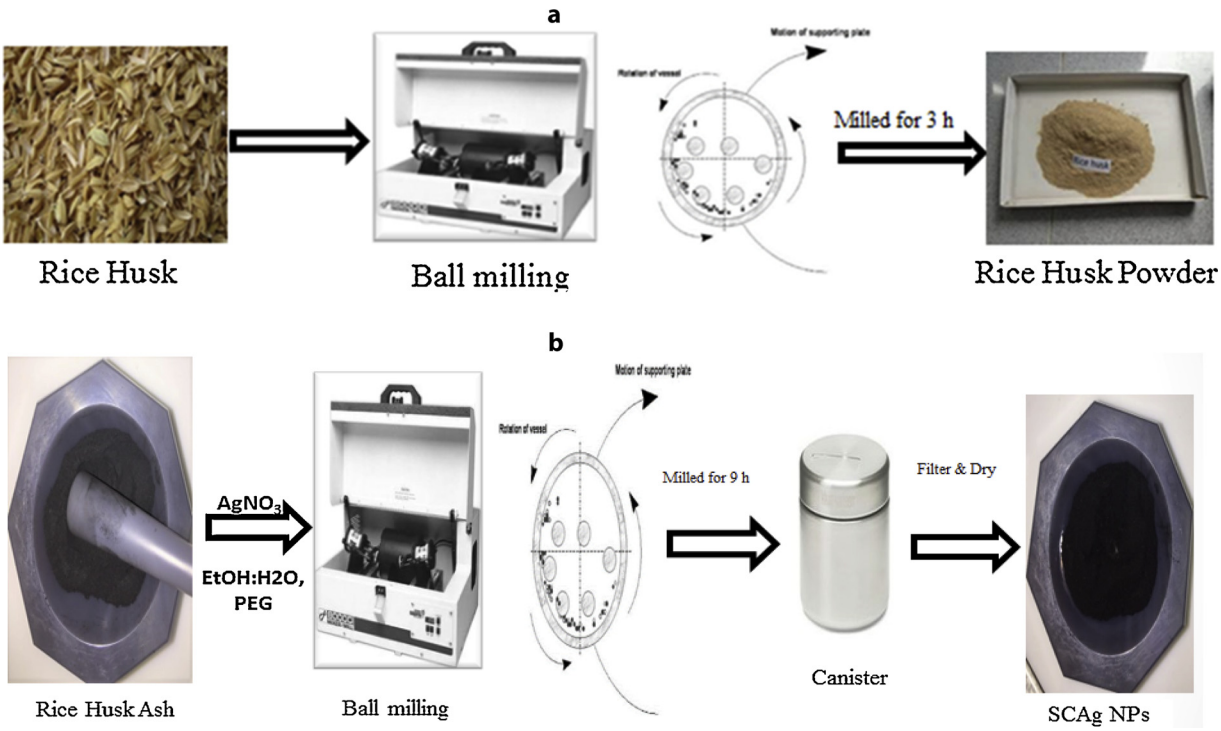

Fig. 1. Flow diagram for preparation of (a) Rice husk powder (RHP) and (b) Si-C-Ag ternary hybrid nanoparticles.

Scientific K-alpha XPS equipped with a hemispherical energy analyzer. A non-monochromatized Al Kα X-ray source was used at 12 keV and 12 mA.

3.5. Field emission scanning electron microscope (FE-SEM)

The morphological analysis of RH ash and fracture surface of nanocomposites thin films was carried out by FE-SEM (Joel JSM -7200 F) equipped with an energy-dispersive X-ray spectrometer. SCAg-NPs and blend composites were placed on a double sided carbon tape and then sputter coated with gold–palladium for 5 min in Hummer 6.2 sputtering system purged with Argon gas and operated at 20 millitorr, 5 V, and 10 milliamps. Film samples were also cut in square shape and placed in the carbon tape, and fractured surface analysis of tensile specimens was also examined by Joel JSM-7200 F.

3.6. Transmission electron microscope (TEM)

The microstructure and particle sizes of the nanoparticles were investigated by Transmission Electron Microscope (TEM-Joel 2010). One (1) mg of the SCAg NPs sample was dispersed in 5 mL of ethanol and sonicated for 10 min in an ultrasonic bath and a drop of the colloidal solution was deposited on a copper grid for analysis.

3.7. Differential scanning calorimetry (DSC)

A TA Q 2000, differential scanning calorimeter (DSC) equipped with the liquid nitrogen cooling system was used to study thermal properties of the nanoparticles, neat polymer, and nanocomposites thin films. Samples of about 15 mg were placed into the aluminum pan and then sealed correctly, and the test runs using an empty reference pan. The sample was first cooled from room temperature to -50 °C at 20.0 °C/min and then heated at -50 °C to 300 °C at 5 °C/min and held at constant temperature for 2.0 min to erase the previous thermal history of the

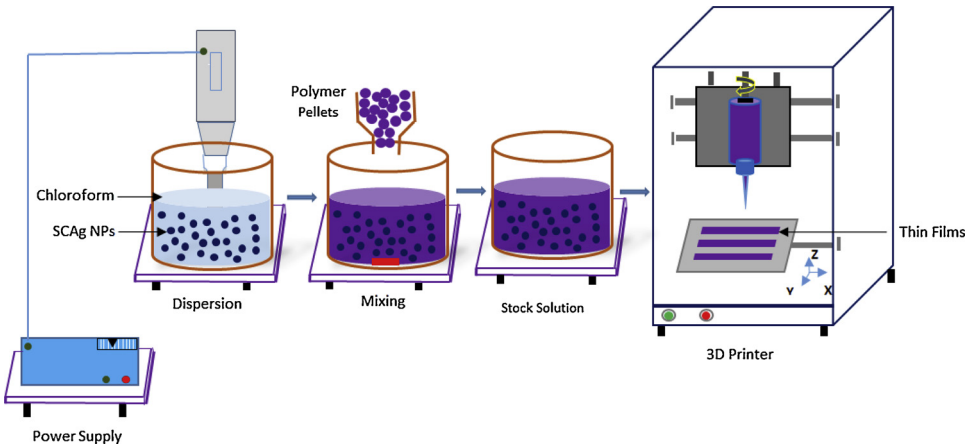

Fig. 2. Schematic diagram of 3D printing process of nanocomposites thin films.

specimen. Then they were again cooled from 300 °C to-50 °C at 20.0 °C/min. After that the sample was again heated from -50 °C to 300 °C at 5.0 °C/min.

3.8. Thermo gravimetric analysis (TGA)

A TA Q 500, thermogravimetric analyzer (TGA) was used to carry out thermogravimetric analysis in the nitrogen atmosphere. Samples of about 15 mg were placed onto platinum pans and heated from 30 °C to 700 °C in a 50 mL flow of N_2. A heating rate of 5 °C/min was used, and the continuous records of sample temperature, mass, first derivative and heat flow were taken.

3.9. Tensile test

Tensile properties of blended nanocomposites thin films were carried out using Zwick Roell Z2.O mechanical testing system. The as prepared samples were dried in vacuum oven at 60 °C for 1 h and then kept in a sealed desiccator until testing. These samples were cut according to the ASTM D 882 dimensions of W: 19 mm x 0.1 mm x L: 120 mm. The tests were carried out at 20 mm gauge length with a crosshead speed of 500 mm/min of 2.5 K N load cells with wedge grips. At least 15 representative samples were tested and most repeated mechanical properties were reported. TestXpert data acquisition software was used to record the data.

3.10. Film preparation for antimicrobial test

The antimicrobial properties of 100 μm thick films fabricated by 3D printing process was investigated on *Salmonella enteritidis* (SE) at 10^1 and 10^5 CFU/ml bacterial concentration and one with full optical density (fod) according to McFarland Standard. To carry out the investigation, lower and higher percentage of silver (0.5 & 1.5%) induced films were cut into 1.5 × 1.5 cm^2 and put them under UV radiation for 15 min. each side in a PCR workstation (Air Clean 600, Serial # 42991). The films were then kept into sterile re-sealable bags (Nasco WHIRL-PAK) until further use.

3.11. Antimicrobial test

The antimicrobial test of the printed films was carried out qualitatively with direct placement of the prepared square films on spots of know concentrations of bacteria. In this study, Mueller Hinton Agar (MHA) and Tryptic Soy Broth (TSB) were used as media. As a representative of foodborne pathogen *Salmonella Enteritidis* (SE) was chosen based on their ability to survive, common prevalence on food and population ability in most food storage temperatures (+4 °C). The Gram-negative bacteria *S. Enteritidis* was incubated at 37 °C for 24 h for this study. Single colonies of bacteria were prepared in TSA plates and 3–5 colonies were transferred into 1.5 mL sterile tubes containing 1 mL TSB using sterile disposable inoculating loops. After that the culture was vortexed and incubated at 37 °C on a shaker at 350 rpm for 3–4 h. Sterile TSB was used to adjust the turbidity of *S. Enteritidis* suspensions to obtain approximately equal optical density (OD) to that of 0.5 McFarland Standard (~1–2 × 10^8 CFU/ml of *E. coli* ATCC 25,922). The OD of the suspension was measured at 600 nm (OD_{600}) using a UV–vis spectrophotometer (Nanodrop 2000c, Wilmington, DE, USA). The starting bacterial concentration was used ranged from 0.095-0.100.

Antimicrobial property of the films was carried out on different inoculated agar surfaces. Approximately 100 μL of the cell suspensions containing the stock (OD_{600}) and 10^1 and 10^5 CFU/mL were dispensed at the center of the agar plates and allowed to air dry under a biosafety hood. The square UV radiated films were then placed directly on the spot on agar plates where the inoculum was dispensed and incubated at required temperature. After 24 h incubation, films were removed with sterile forceps and discarded and the plates were incubated for another 24 h. All plates were visually inspected for any colony growth after 24 h of incubation. Control plates were inoculated with sterile TSB and growth plates were inoculated with specified bacteria species.

3.12. Sample preparation for silver release test

Silver release study was conducted on the fabricated films treated with distill water (DW) and fresh chicken thigh (CT) samples. The release study was carried out by wrapping about 0.5 g of CT with 2 × 2 cm^2 neat, 0.5% and 1.5% Ecoflex/SCAg NPs films. The samples were then stored in the refrigerator at 4 °C for 96 h and 1–4 week. After targeted time interval each sample was removed from the refrigerator, unwrapped the films, cut it into smaller pieces and put it into 50 mL tube. The three CT samples, which were wrapped by neat, 0.5% and 1.5% Ecoflex/SCAg NPs films, were dissolved using ATL tissue lysing buffer and proteinase K enzyme solution. About 360 μL tissue lysing buffer was added followed by 20 μL proteinase K solution was added and vortexed the tube for 30 s using Phenix Benchmis 1000. The tube is then incubated in a water bath (ISOTEMP 220, Fisher Scientific) at 56 °C for 4 h for complete lysis of the CT samples. After that, 15 mL of DW was added to each tube and vortexed for 60 s. The slurry was then filtered with Whatmann 110 mm paper into a 25 mL storage bottle.

On the other hand, silver release test was also carried out on 0.5% and 1.5% Ecoflex/SCAg NPs films. About 0.5 g of each film was immersed in 15 mL DW contained in 25 mL storage bottle and stored in 4 °C in the refrigerator. After targeted time interval the water analyzed for any silver release. Control CT samples were prepared in same way except wrapping with the films. In order to carry out silver release test in AAS, nitric acid was added to each sample to 0.1 M concentration.

3.13. Atomic adsorption spectroscopy (AAS)

Atomic absorption spectroscopy was carried out to investigate the silver concentration in the food samples using Varian AAS 240 (detection limit 0.02 ppm) during release study. The standard samples (0, 2.5, 4, 6, 8 and 10 ppm) were prepared from acidic (2% HNO_3) 1000 g/L Ag AAS standard solution and run as calibration standard before run the samples. In order to determine the silver concentration on the samples, a reference curve was plotted based on calibrated data from the standards. The AAS was run at a wavelength of 328.1 nm, slit width 0.5 nm and lamp current of 4.0 mA using air-acetylene flame to detect silver.

4. Results and discussion

4.1. Materials characterization

4.1.1. X-Ray diffraction and TEM analysis

The XRD pattern of the synthesized SCNPs/Ag nanoparticles is shown in Fig. 3a. The sharp diffraction peak at 22.4° is ascribed to the peak of crystalline cristobalite, SiO_2 which corresponds to the plane (101) with an interlayer spacing of about 0.40 nm. The X-ray patterns of the as synthesized sample is compared with the Jade library Journal of chemical powder diffraction standards (JCPDS) X-ray patterns of cristobalite. As indicated in Fig. 3a the six most prominent characteristic peaks of rice husk sample at 2θ = 22.6°, 25.4°, 32.4°, 36.2°, 51.5° and 56.9° were corresponding to the crystal faces of (101), (111), (102), (200), (112), (202), (212) and (301) of cristobalite with JPCDS card (file No 47-1743) which confirms that the sample is cristobalite, one of the three and most stable phase of silicon dioxide. The prominent characteristic peaks at 2θ = 38.2° & 44.8° corresponding to (111) & (200) crystal planes for silver particles in SCAg NPs. This results confirmed that the *in situ* formation of metallic silver in nano meter scale from silver nitrate through mechnochemical process.

The TEM micrograph in Fig. 3b indicates that the silica particles are 15–100 nm in sizes, highly crystalline and porous. The dark silver particles are embedded in silica particles, are less than 100 nm in size.

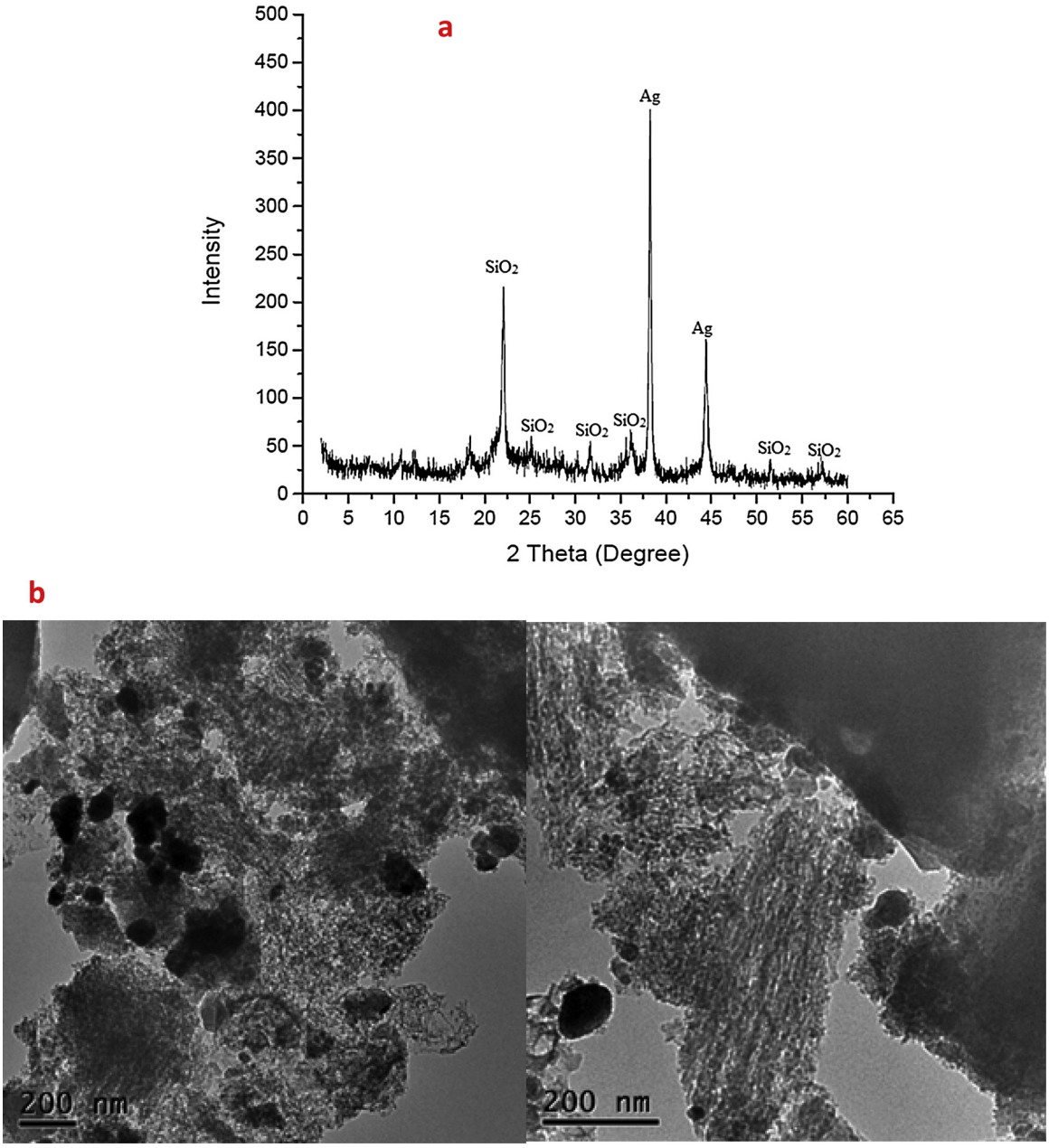

Fig. 3. (a) X-ray diffraction pattern and (b) TEM micrograms of SCAg NPs.

The nano size and porous nature of the particles can facilitate the interactions and bond formation with other materials, can enhance the properties of biopolymer. The incorporation on nano scale silver into silica-carbon hybrid nanoparticles divulges antimicrobial properties into this material and possibilities for a wider range of application such as in antimicrobial paint additives (Sahoo, Kausar, Lee, & Han, 2014), antimicrobial drug (Apalangya, Rangari, Tiimob, Jeelani, & Samuel, 2014) and active packaging filler (Tiimob et al., 2017, 2018).

The morphology of the neat Ecoflex and Ecoflex/SCAg NPs nanocomposites films was characterized by X-ray diffraction, shown in figure S1 (a–e). In figure S1b, the XRD pattern shows the semi-crystalline structure of neat Ecoflex with prominent characteristic peaks at $2\theta = 22.6^{\circ}$, 28.4°, 30.5° and 32.4° with an amorphous background as observed in past studies (Tiimob et al., 2017). As the percentage of SCAg NPs was increasing from 0.5 to 1.5% in the nanocomposite thin films, the XRD patterns exhibited the diffraction peak of crystalline nano silica at $2\theta = 22.4^{\circ}$ and that of silver at $2\theta = 38.2^{\circ}$ shown in Fig. S1(c–e). Similar pattern has been observed in the literature and reported in different studies of silica and biopolymer nanocomposites (Santos, Muller, Grossmann, Mali, & Yamashita, 2014). Crystallinity is responsible for improving the mechanical integrity of various polymer nanocomposites blend (Thuc & Thuc, 2013). The crystalline nature of silica nanoparticles, presence in the polymer matrix does not modify the crystal structure of semi-crystalline PBAT though the percentage of nanoparticles was increased from 0.5 to 1.5 wt. % shown in Fig. S1(c–e). A small addition of nanoparticles compare with the counterpart macro size particles has been found to alter the crystallinity of the polymer matrix. The homogeneously dispersed SCAg nanoparticles in the matrix can further enhance the mechanical properties of the composites films whiles imparting antimicrobial property. However, they can act as nucleating agents, which enhance the formation of large particles with the addition of a higher number of particles and degrade the mechanical properties (Santos et al., 2014). In the literature, it has been found that incorporation of nanoscale materials at lower quantity enhances the inferior properties of the polymer (Pilić et al., 2016; Rahman, Netravali, Tiimob, Apalangya, & Rangari, 2016; Tiimob,

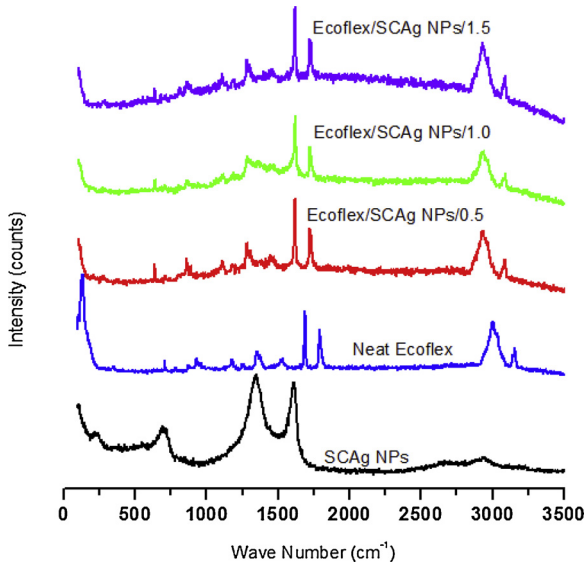

Fig. 4. Raman spectra of (a) SCAg NPs, (b) Neat Ecoflex, (c) Ecoflex/SCAg NPs/0.5, (d) Ecoflex/SCAg NPs/1.0 and (e) Ecoflex/SCAg NPs/1.5.

Jeelani, & Rangari, 2016).

4.1.1.1. Raman spectroscopic analysis. Raman spectroscopic analysis was carried out to understand and nature of functional groups and their interaction with neighboring group. The Raman spectrum shown in figure S2 revealed the presence of carbon in SCAg NPs. As seen in figure S2, the D band Raman shift is in 1330-1380 cm^{-1} range and the G band peak at 1605 cm^{-1} Raman shift. The silicon and silver particles are found at around 210 cm^{-1} and 605 cm^{-1} Raman shift.

Fig. 4 shows the Raman spectra of (a) silica-carbon-silver nanoparticles (SCAg NPs), (b) pristine Ecoflex, (c–e) nanocomposites films at 0.5–1.5 % of SCAg NPs in the region of 100-3500 cm^{-1}. The Raman spectra revealed that distinct vibrational frequencies due to Ecoflex (PBAT) in the blend appeared at 640–860, 1100–1285, 1461, 1618, 1720 and 3085 cm^{-1}. These are due to aromatic ring vibrations and aromatic −C−H stretching, −C═O stretching, $-CH_2$ stretching, aromatic −C═C and −C−O−C stretching in the structure of the soft PBAT polymer respectively (Nar et al., 2014; Vaibhav, Vijayalakshmi, & Roopan, 2015).

The vibrational frequencies in 0.5–1.0 % blend system show a shift by ± 3 to 9 cm^{-1}. This is due to molecular vibration of silica-carbon-silver particles in the blended composite during excitation. The identified bands in blend composite system suggest that there is no strong interaction between the components of the mixture and thereby no new chemical bond is formed between them.

4.1.1.2. BET surface area analyzer. The BET plot of SCAg NPs is shown in Fig. 5 based on the Brunauer-Emmett-Teller (BET) equation. The resulting BET equation is

$$\frac{1}{v\left[\left(\frac{P_\circ}{P}\right)-1\right]} = \frac{c-1}{Vmc}\left(\frac{P}{P_\circ}\right) + \frac{1}{Vmc}$$

Where P and P_0 are the equilibrium and the saturation pressure of adsorbates, v and v_m is the adsorbed and monolayer gas quantity respectively, C is BET constant.

The specific surface area of SCAg NPs was calculated highest surface area 261.025 m^2/g of the nanoparticles according to the following equation:

$$S_{total} = \frac{VmNs}{V}$$

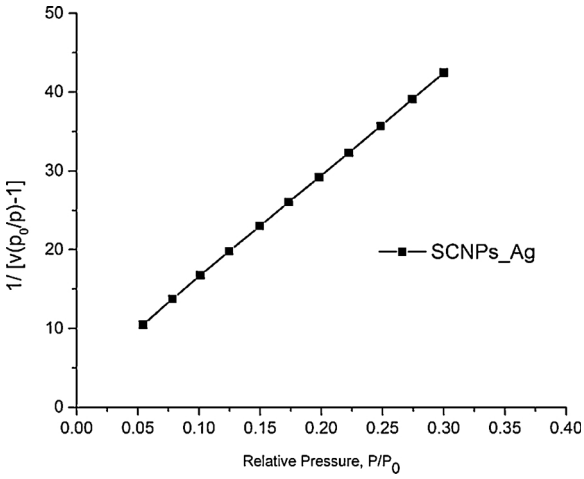

Fig. 5. BET graph of SCAg NPs.

$$S_{BET} = \frac{Stotal}{a}$$

Where N is Avogadro's number, s the adsorption cross section of the adsorbing species, V the molar volume and *a* is the mass of dried sample.

4.1.1.3. X-ray photoelectron spectroscopy. The XPS spectrum revealed the existence of elemental Si, O, and C in the rice husk ash shown in Fig. 6. The binding energy associated with the peaks are 284.29, 532.08, 110.08 and 379.08 eV are assigned to C 1 s, O 1 s, Si 2p and Ag 3d in the nanoparticles, respectively. The composition of C, O, Si and Ag element in SCAg NPs found 46.31%, 37.82%, 10.92% and 0.21% respectively. These results are consistent with literature (Jiang, Kuila, Kim, Ku, & Lee, 2013; Liu, Liu, & Xue, 2004; Park, Seo, Ahn, Kim, & Kang, 2010).

4.1.1.4. Thermal analysis

4.1.1.4.1. Differential scanning calorimetry (DSC). Thermal properties of SCAg NPs and the blended composite fabricated by incorporating 0.5–1.5 % SCAg NPs in Ecoflex (PBAT) polymer matrix are investigated by DSC. The DSC thermograms for the pristine polymer, SCAg NPs and nanocomposites films are shown in the figure S3. The neat PBAT polymer shows glass transition temperature at -32.1 °C and melting temperature at 130.9 °C with a shoulder at around 88.9 °C. The curve for 1.5% blend shows a shift in Tg 48.9 °C–51.2 °C, the highest increase in Tg among other blends. The pristine SCAg NPs showed an endothermic peak at about 128.3 °C due to the

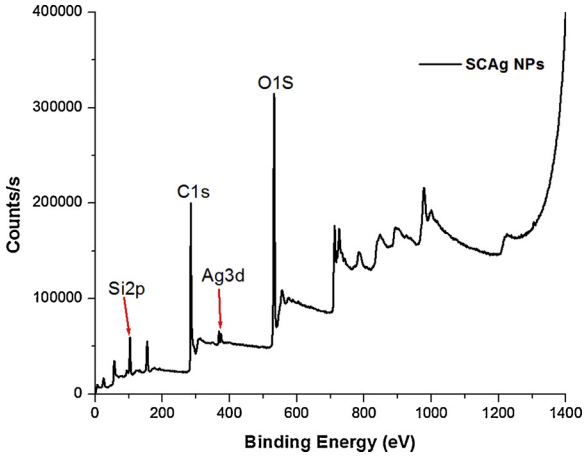

Fig. 6. XPS spectra of rice husk ash SCAg NPs.

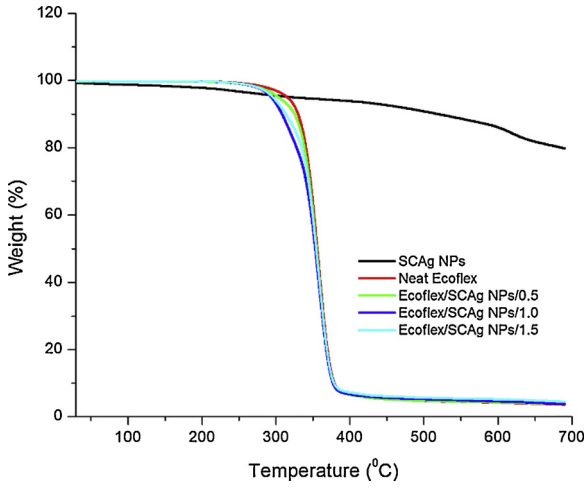

Fig. 7. TGA thermographs of SCAg NPs, Neat Ecoflex and Ecoflex/SCAg NPs nanocomposites films.

decomposition of bonded water which has been confirmed by investigating DSC pattern of the dried SC NPs in previous studies (Chen & Yang, 2015). The uniform dispersion of nanoparticles in the matrix restricts the mobility of polymer chain which increases the glass transition temperature of the polymer as found in previous work (Fukushima, Fina, Geobaldo, Venturello, & Camino, 2012; Kanmani & Rhim, 2014).

4.1.1.4.2. Thermogravimetric analysis (TGA). Thermal stability of pristine Ecoflex, SCAg NPs and their composites thin films at different wt. percentages (0.5 to 1.5%) examined by thermogravimetric analysis are shown in Fig. 7. TGA thermograms showed the weight loss and maximum decomposition temperature of the neat films and the composite films respectively. The amount of remaining material is used to determine the thermal stability of the bio thin films. The pristine SCAg NPs showed almost linear TGA thermograph which leads to enhancing the inferior thermal stability of the polymer. The following improvements observed in the neat and blend systems: onset of degradation, 6 °C and % Residue yield, 1% from the neat system. These improvements are due to the incorporation of thermally stable SCAg NPs into the polymeric blends.

The linear thermogram of pristine SCAg NPs indicates the outstanding thermal stability of ternary blend nanoparticles up to 700 °C (Tiimob et al., 2016). The infusion of SCAg NPs into the polymeric systems at different percentage led to significant enhancement of the thermal stability of the composite films. The thermal stability enhancement can be attributed to the uniformly dispersed silica-carbon-Ag nanoparticles resulted in the decrease of oxygen permeability through the composites. The "zigzag path" effect of this filler materials delay the escape of volatile components degradability in the systems. It is reported in the literature that the well-dispersed organoclay in PBAT matrix increased the barrier effect resulted in the improvement both onset and maximum decomposition temperature. Incorporation of thermally stable nanoparticles into the polymer blends or other materials improve the thermal stability significantly (Peyki, Rahimpour, & Jahanshahi, 2015; Tang et al., 2014). This conforms to our findings with the small addition of SCAg NPs in the PBAT matrix as depicted in Table 1.

4.1.1.5. Spectroscopic analysis

4.1.1.5.1. Scanning electron microscope. Scanning electron microscopic analysis revealed the spheroidal nano silica in the range of 10–100 nm shown in Fig. 8(a & b) from rice husk ash. The energy dispersive spectroscopic (EDS) revealed the presence of silver, silica and carbon particles in the synthesized SCAg-NPs particles shown in Fig. 8(c & d).

4.1.1.6. Mechanical analysis

4.1.1.6.1. Tensile test. The tensile test of pristine Ecoflex films and Ecoflex-SCAg NPs blend nanocomposites is shown in Fig. 9. The following curve is the general mechanical behavior of the polymeric system under tensile load of 2.5 K N. The pristine PBAT composite films showed the satisfactory ductile property. Fig. 9 showed the neat PBAT fails at about 1860% strain. The integration of SCAg NPs with neat polymer at 0.5–1.5 wt. %, the maximum increase of elongation at break and tensile strength found at about 960% strain and 8 N/mm^2 for 1.0 wt. % among the films. But this is a reduction of about 50% strain at maximum loads for incorporation of SCAg NPs compare to the neat system. The highest percentage of stiffness increased for 1.0 wt. % SCAg NPs integration with matrix. In the case of 1.5 wt. % inclusion of SCAg NPs, a significant reduction of ductility of the blend found to 700% strain at break as well as elastic modulus and tensile strength. This is tremendously less than the neat polymeric blend, which implies that the addition of higher concentration of SCAg NPs to the matrix led to the significant compromise in mechanical properties.

4.1.1.7. Fracture surface analysis. Fracture surface analysis after tensile test of the neat and 1.0% Ecoflex/SCNPs nanocomposites thin films were carried out by FE-SEM (Joel JSM 7200 F). The fracture surface SEM micrographs are shown in figure S4. The fractured surface of neat Ecoflex nanocomposites films showed fragile nature during pull out of the films in the tensile test in figure S4 (a, b) at different places. Whereas the fractured surface of 1 wt. % blend system showed an altered morphology (Fig. S4 c and d) with smooth surface and irregular loose polymer fibrils of the matrix which implies the poor adhesion and interfacial interaction of polymer and SCAg NPs in the nanocomposites films. This is also reported in the past studies (Tiimob et al., 2016). The interfacial interaction between the domain and matrix plays the vital role to toughen the composites by diverting the crack paths and delaying the failure of the composite films. In this case, the weakness suggests the poor interaction of metallic silver nanoparticles with polymer matrix.

4.1.1.8. Antimicrobial test

4.1.1.8.1. Antimicrobial study of fabricated films. The antimicrobial property of 3D printed nanocomposites thin films were studied on S. Enteritidis at two different concentrations, at 10^5 CFU/ mL and at full optical density (FOD), as in the McFarland Standard.

The effect on the growth of S. Enteritidis covered with 1.5 × 1.5 cm^2 Ecoflex/SCAg NPs ternary blend nanocomposites films are shown in Fig. 10. In the negative control specimen (Fig.10b_1), a neat active film was placed to cover 100 μL of bacterial concentration (FOD) of the specimen pipetted in the middle of the plate. The control film revealed

Table 1
Thermal profiles of neat and Ecoflex/SCAg NPs nanocomposites thin films.

Specimen	T_{Onset}	T_{d5}	T_{dmax}	%Residue
Neat Ecoflex	326.87 ± 0.72	314.23 ± 1.97	357.26 ± 0.51	3.864 ± 0.13
Ecoflex/SCAg NPs/0.5	332.31 ± 0.98	302.93 ± 0.81	356.72 ± 2.05	3.958 ± 0.07
Ecoflex/SCAg NPs/1.0	328.05 ± 0.11	292.71 ± 0.09	357.26 ± 2.11	4.094 ± 0.08
Ecoflex/SCAg NPs/1.5	330.5 ± 0.79	294.86 ± 1.88	357.8 ± 0.48	4.638 ± 0.05

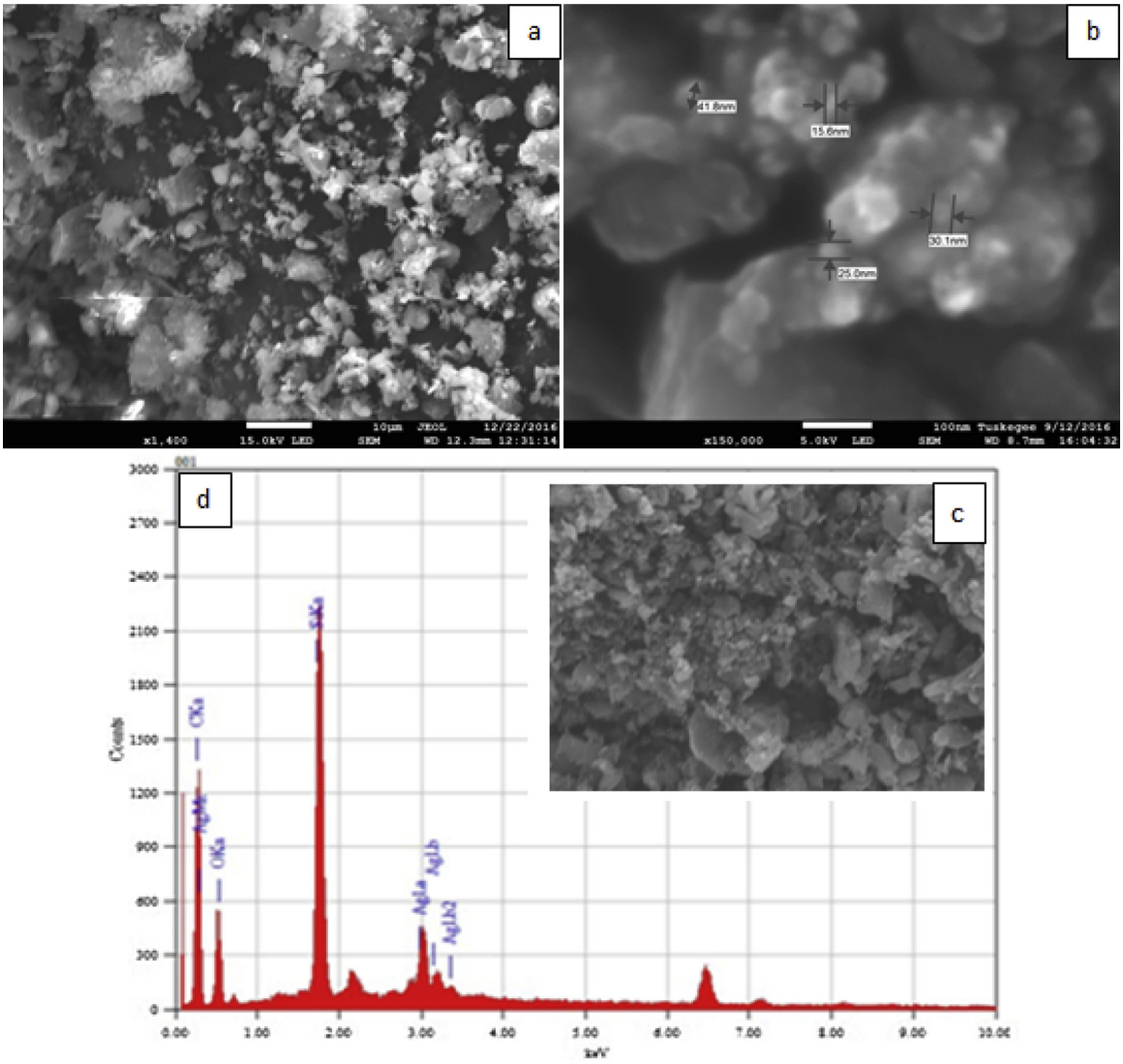

Fig. 8. SEM micrograms of SCNPs/Ag nanoparticles at (a) lower & (b) higher magnification and (c) mapped region for EDS & (d) EDS results.

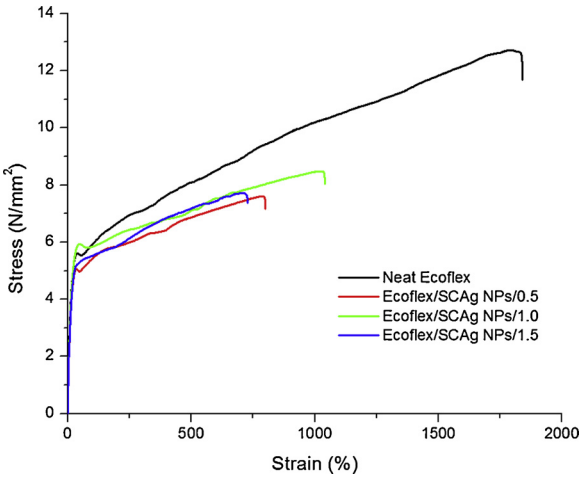

Fig. 9. Stress vs Strain curves of Neat Ecoflex and Ecoflex-SCAg NPs nanocomposites.

that S. Enteritidis grew in the presence of neat film after 24 h incubation (Fig. 10b_2). The bacterial growth increased significantly during further 24 h incubation following film removal (Fig. 10b_3). This implies that the neat film had no antibacterial activity. In another control 100 µL of tryptic soy broth (TSB) was pipetted and incubated for 24 h (Fig. 10a_1-a_2). After incubation the results suggests that there was no bacterial growth in TSB control plate.

When the Ag induced films (0.5 & 1.5%) were placed on the higher and lower concentration of S. Enteritidis, it inhibits the bacterial growth shown in figure 10c_1-c_2, d_1-d_2 respectively. But some growth at the edge of the film (0.5%) at higher concentration (FOD) of S. Enteritidis after 24 h incubation revealed that the bacteriostatic effect of the film could be compromised by very high concentrations. On the other hand, 1.5% Ag induced films showed no bacterial growth in both higher and lower concentration of bacteria. The extended 24 h incubation after film removal (Fig. 10c_4, d_4) showed further bacterial growth means the films are most likely bacteriostatic than bactericidal.

Therefore, this bacteriostatic effect appears to rely on direct contact of the films with bacteria. The main advantage of bacteriostatic effect of the films is to inhibit the bacteria population on contact with time while avoiding issues with antimicrobial agents' contamination due to leaching into food products.

4.1.1.8.2. Silver release study. The silver nanoparticles (Ag NPs) release study was carried out through atomic absorption spectroscopy (AAS) and results are shown in Table 2. The silver release test sample preparation process is shown in Fig. 11.

The silver release study on 3D printed films revealed that there was

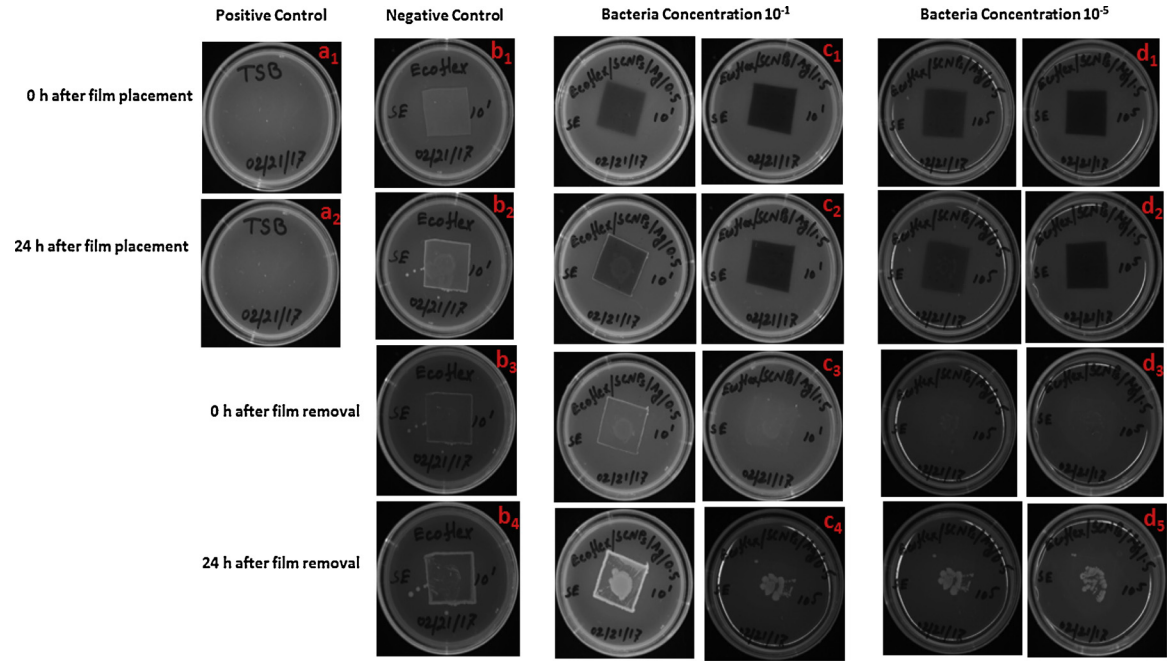

Fig. 10. Antimicrobial effect of Ecoflex/SCAg NPs ternary blend nanocomposites films: (a_1-$a_{2)}$ tryptic soy broth, (b_1-b_4) neat Ecoflex against S. Enteritidis, (c_1-c_4) active films against S. Enteritidis (inoculated at high concentration).

Table 2
Concentration of Silver nanoparticles from fabricated nanocomposites thin films in Distilled Water (DW) and Chicken Thigh (CT).

Specimen	Silver (Ag) concentration, ppm				
	½ week	1 week	2 weeks	3 weeks	4 weeks
Neat film in DW		0	0	0	0
Neat film in CT		0	0	0	0
Ecoflex/SCAg NPs/0.5 film in DW		0	0	0	0
Ecoflex/SCAg NPs/1.5 film in DW		0	0	0	0
Ecoflex/SCAg NPs/0.5 film in CT	0	0	0	0	0
Ecoflex/SCAg NPs/1.5 film in CT	0	0	0	0	0

no silver trace in DW after one (1) week immersion of the lower and higher silver loaded (0.5 & 1.5%) films. It can be inscribed due to the high hydrophobic property of the polymeric system which results no water absorption and thereby no silver release into the water. This result confirmed by past studies (Tiimob et al., 2017).

In case of chicken thigh (CT), the AAS results showed the similar silver release outcomes. The CT samples were packaged in films and stored at 4 °C for 96 h and 1–4 week for the study. This can be ascribed due to very small amount of Ag in the fabricated films. These prolonged studies suggest that Ecoflex/SCAg NPs ternary blend nanocomposites films are encouraging for food packaging applications for extended period devoid of Ag release to the products.

5. Conclusion

In this work, composite films induced with silica-carbon/Ag (SCAg NPs) nanoparticles, prepared through one-step ball milling process, were fabricated by 3D printing process. The nanostructure of the SCAg-NPs was determined by XRD and TEM analysis. Scanning electron microscopic (SEM) analysis also revealed the nanostructure of the synthesized SCAg NPs. Antimicrobial study on fabricated 1.5% Ag induced films showed no bacterial growth in both higher and lower concentration of bacteria. The extended 24 h incubation after film removal showed further bacterial growth means the films are most likely bacteriostatic than bactericidal. Therefore, this bacteriostatic effect appears to rely on direct contact of the films with bacteria. The main advantage of bacteriostatic effect of the films is to inhibit the bacteria population on contact. Based on the results of antimicrobial and silver release study suggests that SCAg NPs composite films has the potential to be used in the field of antimicrobial food packaging applications.

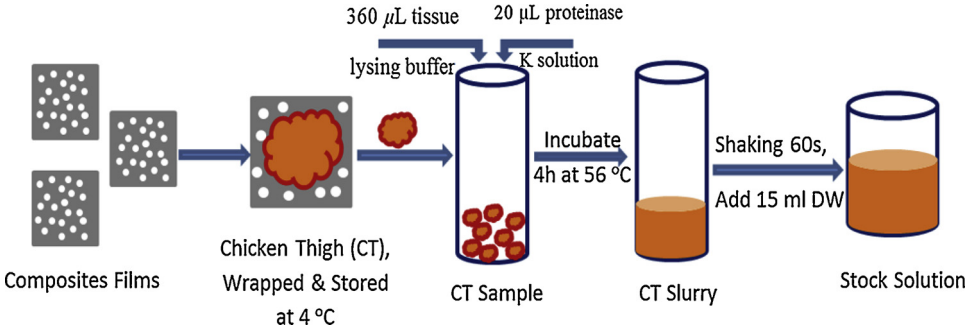

Fig. 11. Schematic diagram of sample preparation for silver release test.

Acknowledgements

The authors would like to acknowledge the financial support of NSF-RISE # 1459007, NSF-CREST# 1735971 and NSF-MRI-1531934 grants. We also would like to acknowledge Dr. Paul Evan, Materials Science and Engineering, Wisconsin for providing the access to XPS facility, Dr. Cheryl D. Colquhoun, Chemistry and Biochemistry, Auburn University for providing the access to AAS facility. The authors are very grateful to Tuskegee University shared instrumentation biomedical research core research facility (NIH grant G12MD007585). Three H's LLC Crossett, Arkansas for supplying rice husk for this study.

Appendix A. Supplementary data

Supplementary material related to this article can be found, in the online version, at doi:https://doi.org/10.1016/j.fpsl.2018.12.003.

References

Apalangya, V., Rangari, V., Tiimob, B., Jeelani, S., & Samuel, T. (2014). Development of antimicrobial water filtration hybrid material from bio source calcium carbonate and silver nanoparticles. *Applied Surface Science. 295*, 108–114.

Balaguer, M. P., Lopez-Carballo, G., Catala, R., Gavara, R., & Hernandez-Munoz, P. (2013). Antifungal properties of gliadin films incorporating cinnamaldehyde and application in active food packaging of bread and cheese spread foodstuffs. *International Journal of Food Microbiology, 166*(3), 369–377.

Beigmohammadi, F., Peighambardoust, S. H., Hesari, J., Azadmard-Damirchi, S., Peighambardoust, S. J., & Khosrowshahi, N. K. (2016). Antibacterial properties of LDPE nanocomposite films in packaging of UF cheese. *LWT-Food Science and Technology, 65*, 106–111.

Beltrán, A., Valente, A. J., Jiménez, A., & Garrigós, M.a. C. (2014). Characterization of poly (ε-caprolactone)-based nanocomposites containing hydroxytyrosol for active food packaging. *Journal of Agricultural and Food Chemistry, 62*(10), 2244–2252.

Chen, J.-H., & Yang, M.-C. (2015). Preparation and characterization of nanocomposite of maleated poly (butylene adipate-co-terephthalate) with organoclay. *Materials Science and Engineering: C, 46*, 301–308.

Fukushima, K., Fina, A., Geobaldo, F., Venturello, A., & Camino, G. (2012). Properties of poly (lactic acid) nanocomposites based on montmorillonite, sepiolite and zirconium phosphonate. *Express Polymer Letters, 6*(11).

Jiang, T., Kuila, T., Kim, N. H., Ku, B.-C., & Lee, J. H. (2013). Enhanced mechanical properties of silanized silica nanoparticle attached graphene oxide/epoxy composites. *Composites Science and Technology, 79*, 115–125.

Kanmani, P., & Rhim, J.-W. (2014). Physical, mechanical and antimicrobial properties of gelatin based active nanocomposite films containing AgNPs and nanoclay. *Food Hydrocolloids, 35*, 644–652.

Li, J., Shirai, T., & Fuji, M. (2013). Rapid carbothermal synthesis of nanostructured silicon carbide particles and whiskers from rice husk by microwave heating method. *Advanced Powder Technology, 24*(5), 838–843.

Liu, P., Liu, W., & Xue, Q. (2004). In situ chemical oxidative graft polymerization of aniline from silica nanoparticles. *Materials Chemistry and Physics, 87*(1), 109–113.

Llana-Ruiz-Cabello, M., Gutiérrez-Praena, D., Puerto, M., Pichardo, S., Moreno, F. J., Baños, A., et al. (2015). Acute toxicological studies of the main organosulfur compound derived from Allium sp. intended to be used in active food packaging. *Food and Chemical Toxicology. 82*, 1–11.

Ma, X., Zhou, B., Gao, W., Qu, Y., Wang, L., Wang, Z., et al. (2012). A recyclable method for production of pure silica from rice hull ash. *Powder Technology, 217*, 497–501.

Marambio-Jones, C., & Hoek, E. M. V. (2010). A review of the antibacterial effects of silver nanomaterials and potential implications for human health and the environment. *Journal of Nanoparticle Research, 12*(5), 1531–1551.

Martínez-Abad, A., Lagaron, J. M., & Ocio, M. J. (2012). Development and characterization of silver-based antimicrobial ethylene–vinyl alcohol copolymer (EVOH) films for food-packaging applications. *Journal of Agricultural and Food Chemistry, 60*(21), 5350–5359.

McCluskey, D. M., Smith, T. N., Madasu, P. K., Coumbe, C. E., Mackey, M. A., Fulmer, P. A., et al. (2009). Evidence for singlet-oxygen generation and biocidal activity in photoresponsive metallic nitride fullerene− polymer adhesive films. *ACS Applied Materials & Interfaces, 1*(4), 882–887.

Moreira, M.d. R., Pereda, M., Marcovich, N. E., & Roura, S. I. (2011). Antimicrobial effectiveness of bioactive packaging materials from edible chitosan and casein polymers: Assessment on carrot, cheese, and salami. *Journal of Food Science, 76*(1).

Nar, M., Staufenberg, G., Yang, B., Robertson, L., Patel, R. H., Varanasi, V. G., et al. (2014). Osteoconductive bio-based meshes based on Poly (hydroxybutyrate-co-hydroxyvalerate) and poly (butylene adipate-co-terephthalate) blends. *Materials Science and Engineering: C. 38*, 315–324.

Palza, H. (2015). Antimicrobial polymers with metal nanoparticles. *International Journal of Molecular Sciences, 16*(1), 2099–2116.

Park, H.-J., Kim, J. Y., Kim, J., Lee, J.-H., Hahn, J.-S., Gu, M. B., et al. (2009). Silver-ion-mediated reactive oxygen species generation affecting bactericidal activity. *Water Research, 43*(4), 1027–1032.

Park, J. T., Seo, J. A., Ahn, S. H., Kim, J. H., & Kang, S. W. (2010). Surface modification of silica nanoparticles with hydrophilic polymers. *Journal of Industrial and Engineering Chemistry. 16*(4), 517–522.

Pelgrift, R. Y., & Friedman, A. J. (2013). Nanotechnology as a therapeutic tool to combat microbial resistance. *Advanced Drug Delivery Reviews, 65*(13–14), 1803–1815.

Peyki, A., Rahimpour, A., & Jahanshahi, M. (2015). Preparation and characterization of thin film composite reverse osmosis membranes incorporated with hydrophilic SiO2 nanoparticles. *Desalination, 368*, 152–158.

Pilić, B. M., Radusin, T. I., Ristić, I. S., Silvestre, C., Lazić, V. L., Baloš, S. S., et al. (2016). Hydrophobic silica nanoparticles as reinforcing filler for poly (lactic acid) polymer matrix. *Hemijska industrija, 70*(1), 73.

Rahman, M. M., Netravali, A. N., Tiimob, B. J., Apalangya, V., & Rangari, V. K. (2016). Bio-inspired “green” nanocomposite using hydroxyapatite synthesized from eggshell waste and soy protein. *Journal of Applied Polymer Science, 133*(22).

Sahoo, P. C., Kausar, F., Lee, J. H., & Han, J. I. (2014). Facile fabrication of silver nanoparticle embedded CaCO 3 microspheres via microalgae-templated CO 2 biomineralization: Application in antimicrobial paint development. *RSC Advances, 4*(61), 32562–32569.

Santos, R. A., Muller, C. M., Grossmann, M. V., Mali, S., & Yamashita, F. (2014). Starch/poly (butylene adipate-co-terephthalate)/montmorillonite films produced by blow extrusion. *Química Nova, 37*(6), 937–942.

Shen, Y., Zhao, P., & Shao, Q. (2014). Porous silica and carbon derived materials from rice husk pyrolysis char. *Microporous and Mesoporous Materials, 188*, 46–76.

Soysal, Ç., Bozkurt, H., Dirican, E., Güçlü, M., Bozhüyük, E. D., Uslu, A. E., et al. (2015). Effect of antimicrobial packaging on physicochemical and microbial quality of chicken drumsticks. *Food Control, 54*, 294–299.

Tang, H., Tu, J.-p., Liu, X.-y., Zhang, Y.-j., Huang, S., Li, W.-z., et al. (2014). Self-assembly of Si/honeycomb reduced graphene oxide composite film as a binder-free and flexible anode for Li-ion batteries. *Journal of Materials Chemistry A, 2*(16), 5834–5840.

Tang, J., Song, Y., Tanvir, S., Anderson, W. A., Berry, R. M., & Tam, K. C. (2015). Polyrhodanine coated cellulose nanocrystals: A sustainable antimicrobial agent. *ACS Sustainable Chemistry & Engineering, 3*(8), 1801–1809.

Thuc, C. N. H., & Thuc, H. H. (2013). Synthesis of silica nanoparticles from Vietnamese rice husk by sol–gel method. *Nanoscale Research Letters, 8*(1), 58.

Tiimob, B. J., Jeelani, S., & Rangari, V. K. (2016). Eggshell reinforced biocomposite—An advanced “green” alternative structural material. *Journal of Applied Polymer Science, 133*(11).

Tiimob, B. J., Mwinyelle, G., Abdela, W., Samuel, T., Jeelani, S., & Rangari, V. K. (2017). Nanoengineered eggshell–silver tailored copolyester polymer blend film with antimicrobial properties. *Journal of Agricultural and Food Chemistry, 65*(9), 1967–1976.

Tiimob, B. J., Rangari, V. K., Mwinyelle, G., Abdela, W., Evans, P. G., Abbott, N., et al. (2018). Tough aliphatic-aromatic copolyester and chicken egg white flexible biopolymer blend with bacteriostatic effects. *Food Packaging and Shelf Life, 15*, 9–16.

Tornuk, F., Hancer, M., Sagdic, O., & Yetim, H. (2015). LLDPE based food packaging incorporated with nanoclays grafted with bioactive compounds to extend shelf life of some meat products. *LWT-Food Science and Technology, 64*(2), 540–546.

Vaibhav, V., Vijayalakshmi, U., & Roopan, S. M. (2015). Agricultural waste as a source for the production of silica nanoparticles. *Spectrochimica Acta Part A: Molecular and Biomolecular Spectroscopy, 139*, 515–520.

Wang, T., Ji, X., Jin, L., Feng, Z., Wu, J., Zheng, J., et al. (2013). Fabrication and characterization of heparin-grafted poly-L-lactic acid–chitosan core–shell nanofibers scaffold for vascular gasket. *ACS Applied Materials & Interfaces, 5*(9), 3757–3763.

Wen, X., Lin, Y., Han, C., Zhang, K., Ran, X., Li, Y., et al. (2009). Thermomechanical and optical properties of biodegradable poly (L-lactide)/silica nanocomposites by melt compounding. *Journal of Applied Polymer Science, 114*(6), 3379–3388.

Yuvakkumar, R., Elango, V., Rajendran, V., & Kannan, N. (2014). High-purity nano silica powder from rice husk using a simple chemical method. *Journal of Experimental Nanoscience, 9*(3), 272–281.